BJP British Journal of Pharmacology

DOI:10.1111/j.1476-5381.2011.01723.x
www.brjpharmacol.org

RESEARCH PAPER

Using microdialysis to analyse the passage of monovalent nanobodies through the blood–brain barrier

G Caljon[1,2,3], V Caveliers[4], T Lahoutte[4], B Stijlemans[2,3], GH Ghassabeh[2,3], J Van Den Abbeele[1], I Smolders[5], P De Baetselier[2,3], Y Michotte[5], S Muyldermans[2,3], S Magez[2,3] and R Clinckers[5]

[1]*Department of Animal Health, Unit of Veterinary Protozoology, Institute of Tropical Medicine Antwerp, Antwerp, Belgium,* [2]*Unit of Cellular and Molecular Immunology, Vrije Universiteit Brussel, Brussels, Belgium,* [3]*Department of Molecular and Cellular Interactions, VIB, Brussels, Belgium,* [4]*Department of Nuclear Medicine, UZ Brussel and In Vivo Cellular and Molecular Imaging, ICMI, Vrije Universiteit Brussel, Brussels, Belgium, and* [5]*Department of Pharmaceutical Chemistry and Drug Analysis, Center for Neuroscience, Vrije Universiteit Brussel, Brussels, Belgium*

Correspondence
Ralph Clinckers, Center for Neuroscience Vrije Universiteit Brussel, Department of Pharmaceutical Chemistry and Drug Analysis, Vrije Universiteit Brussel, Laarbeeklaan 103, 1090 Brussels, Belgium. E-mail: ralph.clinckers@vub.ac.be

Keywords
nanobody; brain perfusion; blood–brain barrier; microdialysis; single photon emission computed tomography; inflammation; trypanosomiasis

Received
12 May 2011
Revised
28 August 2011
Accepted
18 September 2011

BACKGROUND AND PURPOSE

Nanobodies are promising antigen-binding moieties for molecular imaging and therapeutic purposes because of their favourable pharmacological and pharmacokinetic properties. However, the capability of monovalent nanobodies to reach targets in the CNS remains to be demonstrated.

EXPERIMENTAL APPROACH

We have assessed the blood–brain barrier permeability of Nb_An33, a nanobody against the *Trypanosoma brucei brucei* variant-specific surface glycoprotein (VSG). This analysis was performed in healthy rats and in rats that were in the encephalitic stage of African trypanosomiasis using intracerebral microdialysis, single photon emission computed tomography (SPECT) or a combination of both methodologies. This enabled the quantification of unlabelled and ^{99m}Tc-labelled nanobodies using, respectively, a sensitive VSG-based nanobody-detection ELISA, radioactivity measurement in collected microdialysates and SPECT image analysis.

KEY RESULTS

The combined read-out methodologies showed that Nb_An33 was detected in the brain of healthy rats following i.v. injection, inflammation-induced damage to the blood–brain barrier, as in the late encephalitic stage of trypanosomiasis, significantly increased the efficiency of passage of the nanobody through this barrier. Complementing SPECT analyses with intracerebral microdialysis improved analysis of brain disposition. There is clear value in assessing penetration of the blood–brain barrier by monovalent nanobodies in models of CNS inflammation. Our data also suggest that rapid clearance from blood might hamper efficient targeting of specific nanobodies to the CNS.

CONCLUSIONS AND IMPLICATIONS

Nanobodies can enter the brain parenchyma from the systemic circulation, especially in pathological conditions where the blood–brain barrier integrity is compromised.

Abbreviations

µCT, micro computed tomography; aCSF, artificialCSF; IA, injected activity; MPI, mean pixel intensity; Nb, nanobody; ROI, region of interest; SPECT, single photon emission computed tomography; V_H, variable domain of the heavy chain of an antibody; V_{HH}, variable domain of the heavy chain of a heavy-chain antibody; VSG, variant-specific surface glycoprotein

Introduction

African trypanosomes are extracellular protozoan parasites, transmitted by the tsetse fly and cause human African trypanosomiasis (HAT, also known as sleeping sickness) and livestock trypanosomiasis in sub-Saharan Africa. During the course of infection, trypanosomes thwart the host antibody response by using antigenic variation; hierarchically expressing a single member of a large repertoire of variant specific glycoprotein (VSG) proteins, the major antigenic target in this organism (Barry and Mcculloch, 2001; Vanhamme *et al.*, 2001). Adding to this parasite's evasion of the host immunity, the molecular organization of 5×10^6–10^7 VSG copies per cell as densely packed surface dimers (Auffret and Turner, 1981) results in a cryptic topography of the invariant surface epitopes, which are inaccessible to conventional antibodies (Zamze *et al.*, 1991). Alternative targeting moieties that are not limited by accessibility at this scale are nanobodies, antigen-binding V_H fragments of approximately 15 kDa, derived from *Camelidae* heavy-chain antibodies (HcAbs) (Hamers-Casterman *et al.*, 1993). Using phage display and affinity panning strategies (Lauwereys *et al.*, 1998; Nguyen *et al.*, 2001), several antigen-binding nanobodies were previously selected from a phagmid library that was generated from a VSG-immunized camel (Stijlemans *et al.*, 2004). One of these nanobodies, Nb_An33, recognizes a VSG epitope on *Trypanosoma brucei brucei* AnTat1.1 (Stijlemans *et al.*, 2004). Several other nanobodies that target epitopes on trypanosome surface proteins have been identified, some of which exert direct *in vitro* and *in vivo* trypanolytic activity, independent of the activation of complement (Stijlemans *et al.*, 2011). Clearly, nanobodies have potential applications in diagnosis and drug delivery (Stijlemans *et al.*, 2004; Baral *et al.*, 2006; Saerens *et al.*, 2008).

In spite of these preclinical advances in nanobody technology, as applied to African trypanosomiasis, several problems remain to be overcome if nanobody-based approaches are to be considered as putative therapies. A major problem is the progression of human African trypanosomiasis (caused by *T. b. gambiense* and *T. b. rhodesiense)* from a haemolymphatic to an encephalitic stage, which imposes several restrictions on drug use (Kennedy, 2004). The currently available drugs for this second-stage human trypanosomiasis are limited to the trivalent organo-arsenical compounds, melarsoprol and eflornithine (DFMO or DL-α-difluoromethylornithine), which can cause significant side effects (see Fairlamb, 2003 and Kennedy, 2004). Recently, combination therapy with eflornithine and nifurtimox, a licensed drug against Chagas disease, has been recommended as a first-line treatment against second-stage *T. b. gambiense* infection (Priotto *et al.*, 2009; Yun *et al.*, 2010).

During the progression of infection, parasites gain access to the CNS in two waves, as elucidated from experimental rodent models (see Kristensson *et al.*, 2010 and Rodgers, 2010). In a first wave, parasites pass through fenestrated vessels and gain access to the choroid plexus, the dorsal root ganglia and circumventricular organs (Schultzberg *et al.*, 1988). This is followed by a second, multistep process that occurs at the post-capillary venules. There, a parasite-derived cathepsin L-like cysteine protease (brucipain) (Nikolskaia *et al.*, 2006) and inflammation-induced modifications (Masocha *et al.*, 2004) putatively weaken tight junctions and induce laminin filament remodelling in the endothelial basement membrane, favouring parasite infiltration into the perivascular space. From there, IFN-γ-dependent mechanisms that involve MMPs and CXCL10 facilitate the passage of parasites and leukocytes through the *glia limitans* into the brain parenchyma (Masocha *et al.*, 2004; Amin *et al.*, 2009). Previous histological and imaging studies have documented mild oedema during the encephalitic stage of infection, and the blood–brain barrier is more permeable to tracers such as rhodamine with observable infiltration in several brain regions, especially in the choroid plexus and Ammon's horn in the hippocampus (Philip *et al.*, 1994). However, despite the blood–brain barrier damage that occurs during this stage, several anti-trypanosomal drugs such as suramin and pentamidine are ineffective in clearing parasites from the CNS (see Fairlamb, 2003).

The ability of monovalent nanobodies to cross the blood–brain barrier when this barrier has been affected by the acute brain inflammation during the encephalitic stage of trypanosomiasis has not yet been assessed. Here, we have developed a method combining single photon emission computed tomography (SPECT) and intracerebral microdialysis to assess the concentration of active nanobody in the hippocampus. This brain region shows increased dye infiltration during the encephalitic phase of trypanosomiasis (Philip *et al.*, 1994) and can be reproducibly studied by microdialysis. Using SPECT and microdialysis technologies, we have found that increased damage to the blood–brain barrier, during the infection increased penetration of nanobody into the brain. However, the concentrations that were detected in the brain parenchyma remain below the therapeutically active level, which is likely to result from the rapid clearance rates of these monovalent nanobodies from blood.

Methods

Nb_An33 purification and ^{99m}Tc labelling

A fusion protein of Nb_An33 and the pelB leader sequence, designed to drive export to the periplasm via the secretory (*sec*) pathway, was expressed using a Lac promotor in *Escherichia coli* WK6 cells (Stijlemans *et al.*, 2004). Nanobody was purified from periplasmic extracts as described earlier (Conrath *et al.*, 2001). Briefly, the 6×histidine-tagged Nb_An33 was absorbed onto a Ni-NTA column (Qiagen, Venlo, the Netherlands) and eluted using 0.5 M imidazole. The protein was further purified by gel filtration on a Superdex 75 HR10/30 column connected to an Äkta Explorer (GE Healthcare, Diegem, Belgium) with PBS as running buffer. Nb_An33 concentrations were determined by spectrophotometry, and aliquots were stored at –20°C until further use.

Purified Nb_An33 was labelled with ^{99m}Tc at the His_6 tail, as described previously (Gainkam *et al.*, 2008; Huang *et al.*, 2008). Briefly, $[^{99m}Tc(H_2O)_3(CO)_3]^+$ was synthesized by adding 1 mL of fresh $^{99m}TcO_4^-$ eluate (0.74–3.7 GBq) from a ^{99}Mo–^{99m}Tc generator (Drytec; GE Healthcare) to an Isolink kit (Mallinckrodt Medical BV, Petten, the Netherlands); the mixture was boiled for 20 min. After neutralization with 1 N HCl, $[^{99m}Tc(H_2O)_3(CO)_3]^+$ was added to a 1 mg·mL^{-1} solution of nanobody and was incubated for 60 min at 50°C. After this

labelling step, the ^{99m}Tc-nanobody solution was purified on a NAP-5 gel filtration column (GE Healthcare) pre-equilibrated with PBS to remove unbound $[^{99m}Tc(H_2O)_3(CO)_3]^+$ and passed through a 0.22 μm Millipore filter to eliminate possible aggregates. The labellling efficiency and radiochemical purity were assessed by instant thin-layer chromatography (ITLC) using 100% acetone as the mobile phase, followed by radiometric chromatogram scanning (VCS-201, Veenstra, the Netherlands).

Animals and parasite strains

All animal care and experimental protocols complied with the European Guidelines on Animal Experimentation and were approved by the Ethical Committee of the Faculty of Medicine of the Vrije Universiteit Brussel (ref. 07-220-5).

Parasites for VSG purification were expanded in in-house bred 6 to 8 week-old C57Bl/6 mice. All rat experiments were conducted in male albino Wistar rats (Iffa Credo, Brussels, Belgium), with or without infection by the pleomorphic *T. b. brucei* AnTat1.1E strain (Institute of Tropical Medicine, Antwerp, Belgium). The rats were housed in groups under standard environmental conditions (temperature 21°C, humidity 60%, 10/14 h dark/light cycle, lights on at 0700 h). Rats were infected when they weighed 100–150 g by an i.p. injection of 2.5×10^4 parasites in 500 μL RPMI 1640 (Invitrogen, Merelbeke, Belgium). Parasitaemia was determined by counting parasites in a 2.5 μL blood sample diluted 1:200 in PBS using a light microscope and a Bürker haematocytometer. In parallel, control animals received an i.p. injection of 500 μL RPMI. Infected and control rats weighed between 280 and 360 g at the time of the imaging/microdialysis experiments. From earlier data, *T. b. brucei* AnTat1.1E parasites appear in the rat brain parenchyma by 16 days post infection (dpi) (Amrouni *et al.*, 2010) and in murine models the blood–brain-barrier shows significant damage by 28 dpi, increasing in the terminal stages of the disease (Philip *et al.*, 1994; Sanderson *et al.*, 2008; 2009; Rodgers *et al.*, 2011).

For our analyses, rats were divided in three experimental groups based on the duration of infection and the degree of parasitaemia: (i) control animals 29–30 days post-sham infection; (ii) animals in the early encephalitic stage with $<2 \times 10^6 \cdot mL^{-1}$ parasites in the peripheral blood (i.e. 25–26 dpi); and (iii) animals in the late/terminal encephalitic stage with high parasitaemia ($>2 \times 10^8 \cdot mL^{-1}$) in the peripheral blood (i.e. 29–30 dpi).

Surgery

Rats were anaesthetized with a mixture of ketamine–HCl (90.5 $mg \cdot kg^{-1}$; Ceva, Libourne, France) and diazepam (Roche, Brussels, Belgium; 4.5 $mg \cdot kg^{-1}$). A MAB 6.14.IC guide cannula with a replaceable inner guide (MAB Microbiotech, Stockholm, Sweden) was implanted stereotactically in the hippocampus, 3 mm above the final probe membrane position (CA1–CA3 region). The coordinates were 4.6 mm lateral and 5.6 mm posterior to bregma and 4.1 mm ventral starting from the dura (Paxinos and Watson, 1986). The cannula was fixed to the skull with dental acrylic cement. Post-operative analgesia was assured by a single injection of ketoprofen (4 $mg \cdot kg^{-1}$ i.p.; Merial, Belgium). Immediately after surgery, the guide cannula obturator was replaced with a sterile MAB 2.14.3 [3 mm 35 kDa cut-off polyethersulphone (PES) membrane] microdialysis probe (MAB Microbiotech). These microdialysis probes are non-metal probes with an inlet/outlet made from polyether ether ketone (PEEK) and a probe shaft made from polyimide tubing. The probes are continuously perfused with aCSF/0.5% BSA at a constant flow rate of 0.5 $\mu L \cdot min^{-1}$ (CMA 100 microdialysis pump, CMA Microdialysis, Solna, Sweden). Following surgery, the animals were housed individually in experimental cages with access to water and standard laboratory chow *ad libitum*. Microdialysis probe positioning in the hippocampus was histologically verified using haematoxylin staining.

Experimental microdialysis protocols

Dialysate sampling was started after a minimum period of 16 h following the completion of surgery, permitting the animals to recover.

Protocol 1: Microdialysis probe recovery. The recovery of the dialysis membranes was determined *in vivo* for all compounds under investigation using the retrodialysis method (Wang *et al.*, 1993) to calculate the actual extracellular fluid concentrations from the determined microdialysate concentrations. Each experiment started with the collection of a 2 h blank sample during which blank aCSF/0.5% BSA was perfused. Subsequently, according to the retrodialysis approach, the microdialysis probe was perfused with known concentrations (C_{in}) of either Nb_An33 (500 $ng \cdot mL^{-1}$), ^{99m}Tc-Nb_An33 (37 MBq), ^{99m}Tc-Sestamibi (37 MBq) or Evans Blue (500 $ng \cdot mL^{-1}$) for three periods of 120 min. The disappearance of the drug is monitored by determining the microdialysate concentrations (C_{out}). The probe recovery is then computed as the ratio of drug lost during passage ($C_{in} - C_{out}$) and drug entering the microdialysis probe (C_{in}).

Protocol 2: Pinhole SPECT/Micro-CT imaging combined with intracerebral microdialysis. After a blank microdialysate collection of 40 min, yielding 20 μL microdialysate (0.5 $\mu L \cdot min^{-1}$ perfusion rate), ^{99m}Tc-Sestamibi was injected via the lateral tail vein into conscious rats. The total injected activity was individually determined (mean ± SD: 122 ± 40 MBq, $n = 12$). Three min later, anesthesia was induced by i.p. injection of 100 $mg \cdot kg^{-1}$ pentobarbital (Ceva, Libourne, France). Rats were placed in supine position on a bed with their head firmly fixed between two circular disks containing three ^{57}Co point sources (Canberra, Zellik, Belgium). This bed can be interchanged between μCT and μSPECT. The six beads provided reference points in both image modalities and were used as fiducial markers to generate a spatial transformation matrix (Vanhove *et al.*, 2009). After 7 min, μSPECT acquisitions were performed using a dual-headed gamma camera (e.cam180 Siemens Medical Solutions, Wheaton, IL, USA) equipped with a 1 mm pinhole collimator (focal length 250 mm; 257 mm radius of rotation) (Nuclear Fields, Vortum-Mullem, the Netherlands). Sixty-four projections, each 40 s, were acquired over 360° of rotation into a 128 × 128 matrix with a zoom factor of 1. The total imaging time was 30 min. During the whole procedure (^{99m}Tc-Sestamibi injection, anaesthesia induction and SPECT acquisition) a second 20 μL microdialysate was collected. At the end of the μSPECT acquisition, a free ^{99m}Tc-

tricarbonyl solution of approximately 185 MBq was retrodialysed at a flow rate of 0.5 μL·min^{-1} via the inlet of the microdialysis probe, followed by a 2 min μSPECT acquisition. Following the μSPECT acquisition, μCT images were acquired using a SkyScan 1178 high-throughput *in vivo* μCT system (SkyScan, Kontich, Belgium). X-ray projection images were acquired into an 85 × 85 matrix at 50 kV and 615 μA. By means of two X-ray detector-source pairs, 96 projections were acquired over 180°, with total acquisition time of 2 min. The same procedure was followed for SPECT/CT analysis following i.v. ^{99m}Tc-Nb_An33 injection (mean ± SD: 119 ± 41 MBq, n = 12).

Protocol 3: Intracerebral microdialysis. Microdialysis probe implantation was performed as described above, followed by a 16–18 h recovery period. The probe was continuously perfused at a work flow rate of 0.5 μL·min^{-1} with aCSF/0.5%BSA. Conscious rats received an i.v. injection via the lateral tail vein with a combination of Nb_An33 (4 mg·kg^{-1}) and ^{99m}Tc-Sestamibi (mean ± SD: 119 ± 43 MBq, n = 18) or ^{99m}Tc-Nb_An33 (mean ± SD: 126 ± 36 MBq, n = 21). The total injected activity was individually determined. Microdialysates were collected for 2 h. After a 1 h wash-out period, a second i.v. Nb_An33 (4 mg·kg^{-1}) injection was given followed by a second 2 h microdialysis collection period. Dialysates were analysed for Nb_An33, ^{99m}Tc-Sestamibi and ^{99m}Tc-Nb_An33 content using an ELISA technique and a γ-counter respectively. Following the first infusion, rats received a 2 mL i.v. injection of 0.5% Evans Blue in PBS, followed by a final 2 h microdialysis sampling period. The final dialysate was analysed using a spectrophotometric method for Evans Blue quantification.

Rats were subsequently killed and perfused transcardially with 4% paraformaldehyde in 0.1 M phosphate buffer, pH 7.4. The brains were removed and post-fixed overnight in the same fixative solution and then placed in 30% sucrose for cryoprotection, frozen in powdered dry ice and stored at –80°C. Coronal brain sections (50 μm) were prepared with a cryostat (Microm HM 525, MICROM International, Walldorf, Germany) and mounted onto glass slides for fluorescence microscopic detection of Evans Blue distribution in the tissue surrounding the probe implantation site and the contralateral side.

Spectrophotometry and fluorescence microscopy for Evans Blue analysis in microdialysates and brain slices

The presence of Evans Blue in the microdialysates was quantified by spectrophotometry at 655 nm in microtiter plates. Concentrations were determined in comparison with a standard 1/10 dilution series starting from 0.05% Evans Blue in aCSF with 0.5% BSA. Evans Blue brain uptake was expressed as the mean percentage of injected mass (%IM) recovered in the microdialysate samples.

Distribution of Evans Blue in the brain tissue slides was analysed on a Zeiss Axio Imager microscope equipped with the Zeiss filter set 15 (excitation: BP 546/12, beam splitter: FT 580, emission: LP 590). Digital images were made with a 5× objective lens from the brain regions ipsilateral and contralateral to the probe implantation site. Mean fluorescence intensities were determined by image analysis in the Adobe Photoshop CS (version 8.0) program. For each rat, at least six slides were prepared, from which two non-overlapping images of the ipsilateral and contralateral sides were analysed. The fluorescence microscopy data are expressed as the mean pixel intensity (MPI) for each hemisphere or experimental group.

Radioactivity measurements for 99mTc-Nb_An33 and 99mTc-Sestamibi analysis in microdialysates and blood samples

^{99m}Tc-labelled Nb_An33 and ^{99m}Tc-Sestamibi in the microdialysate and blood samples were measured against a standard of known radioactivity using an automated γ-counter (Cobra II Inspector 5003, Canberra Packard, Zellik, Belgium) and corrected for decay. Counts lower than 1000 cpm (counts per minute) were considered as background. Brain uptake was calculated as percentage of injected activity (% IA) recovered in the microdialysate corrected for decay for each animal. In addition, ITLC was performed on microdialysates samples as described before, in order to evaluate whether the radioactivity recovered was attributed to either intact ^{99m}Tc-Nb_An33 or free ^{99m}Tc.

In a separate group of rats, blood samples were collected from the tail vein at 1, 5, 10, 20, 30, 60, 90 and 120 min post injection of ^{99m}Tc-Nb_An33 (mean ± SD: 48 ± 20 MBq, n = 6) or ^{99m}Tc-Sestamibi (mean ± SD: 61 ± 45 MBq, n = 6) in control rats and rats 29–30 days post infection to obtain a time activity blood curve. Blood sample radioactivity was expressed as % injected activity in the total blood volume (%IA/BV), corrected for decay. The blood volume (BV) was calculated in relation to body weight (BW) using the experimentally determined equation of Lee and Blaufox (1985): BV = 0.06 × BW + 0.77.

μSPECT/CT Image analysis

The μCT images were reconstructed using the software provided by the scanner manufacturer (Vanhove *et al.*, 2009). Image viewing and quantification were performed using AMIDE (Medical Image Data Examiner) software (Loening and Gambhir, 2003). Fusion of the first functional μSPECT image and the anatomical μCT image (Figure S1A) allows accurate localization and quantification of the tracer in the brain. Fusion of the second μSPECT image (Figure S1B), acquired during the retrodialysis procedure, with the μCT image allows visualization and identification of a three-dimensional ellipsoid region of interest (ROI) corresponding to the probe membrane position and dialysis area (Figure S1C,D). The same ROI was transposed to the contralateral side to determine radioactivity counts in the brain region without probe implant (Figure S1E). Corrections were made for attenuation and scatter (Meikle *et al.*, 2005; Vanhove *et al.*, 2009; Hernot *et al.*, 2010). ^{99m}Tc-Nb_An33 and ^{99m}Tc-Sestamibi brain uptake was calculated as the counts in the tissue divided by the IA and normalized for the ROI size (%IA·cm^{-3}). The values of the contra- and the ipsilateral hemisphere were compared to investigate the impact of microdialysis probe implantation on blood–brain barrier functionality.

VSG-specific ELISA for Nb_An33 analysis in microdialysates

The soluble form of the *T. b. brucei* AnTat1.1 VSG (sVSG) was purified as described elsewhere (Lanham and Godfrey, 1970; Cross, 1975) to serve as coating antigen in ELISA. Briefly, C57B1/6 mice were injected with 5000 monomorphic AnTat1.1 parasites. Five to seven days later, heparinized blood was collected, and the parasites were isolated by DEAE-52 anion-exchange chromatography (Lanham and Godfrey, 1970). Parasites were subjected to a heat and pH shock, resulting in sVSG release into the supernatant (Cross, 1975). Soluble VSG was further purified by Resource Q anion exchange chromatography and gelfiltration on a Superdex 75 HR10/30 column (Lanham and Godfrey, 1970; Cross, 1975). The purity of the sVSG was analysed by SDS-PAGE and Coomassie staining combined with Western blot using a rabbit anti-VSG polyclonal antiserum. All sVSG samples were stored at –20°C until further use.

In order to determine Nb_An33 concentrations in the collected microdialysates, a VSG-based nanobody detection ELISA was optimized. For that purpose, Immunosorb plates (Nunc) were coated with 200 ng purified sVSG per well in 0.1 M $NaHCO_3$ (pH 8.3) and blocked with 0.5% BSA in PBS. Microdialysates and a standard Nb_An33 serial 1:2 dilution series (prepared in aCSF with 0.5% BSA) were loaded onto the plates, followed by nanobody detection using a peroxidase-conjugated mouse anti-His Tag IgG (Serotec, MCA1396P) and 3,3′,5,5′-tetramethylbenzidine as substrate. Optical densities were measured at 450 nm after stopping the reaction by adding H_2SO_4 to a final concentration of 0.33 M. Nb_An33 concentrations in the dialysates were determined based on the standard curve and are expressed as the mean percentage of the total injected mass (%IM) recovered in the microdialysate samples.

Statistical analysis

All data in text are expressed as mean ± SD; data in Figures are shown as box and whisker plots with median, quartiles and ranges or as mean ± SD, as indicated. GraphPad Instat software was used for statistical analysis. A Kruskal–Wallis test, followed by Dunn's multiple comparisons *post hoc* analysis, was performed for comparison of the mean values between groups. A Wilcoxon matched-pairs signed ranks test was used for comparison of the mean values between the ipsilateral and contralateral side within one group. All statistical tests were performed at the 5% level of significance.

Materials

Compounds used throughout the experiments were a nanobody (Nb_An33) against the *T. b. brucei* AnTat1.1 VSG, the control tracers Evans Blue (Sigma-Aldrich, St. Louis, MO, USA) and ^{99m}Tc-Sestamibi (^{99m}Tc-labelled 2-methoxy-isobutyl-isonitrile; Cardiolite, Bristol-Myers-Squibb, Princeton, NJ, USA), prepared according to the manufacturer's instructions. The aqueous perfusion medium for the microdialysis experiments was made with deionized water (Seralpur pro 90 CN, Belgolabo, Overijse, Belgium) and filtered through a 0.2 µm membrane filter. It consisted of artificial CSF (aCSF) (composition in mM: NaCl 147, $MgCl_2$ 1.0, $CaCl_2$ 1.2, KCl 2.7, ascorbic acid 0.2 in a 2 mM phosphate buffer pH 7.4) with 0.5% BSA. BSA was added to prevent water loss from the microdialysis probe. BSA also functions as a carrier molecule as it minimizes sticking of peptides to the dialysis membrane and connecting tubing (Trickler and Miller, 2003). Nb_An33, Evans Blue and ^{99m}Tc-Sestamibi were dissolved in physiological saline for i.v. injection.

Results

Parasitaemia and disease course

Wistar rats, infected with *T. b. brucei* AnTat1.1E, displayed a classical parasitaemia pattern with neurological complications in the encephalitic stage as described earlier (Darsaud *et al.*, 2003; Chevrier *et al.*, 2005; Amrouni *et al.*, 2010). After an asymptomatic period, infected rats displayed a decreased body weight gain and increasingly more obvious signs of morbidity, including hypo-activity (sensory and locomotor) and dull fur. Towards the lethal phase of the infection (29–35 days post infection), rats became severely anemic and carried a heavy parasitic load. In addition, rats in the encephalitic stage of infection became increasingly more susceptible to the anesthesia that was used during the microdialysis probe implantation.

Microdialysis probe recovery

Each microdialysis result was corrected for *in vivo* probe recovery determined by retrodialysis. The *in vivo* microdialysis probe recoveries used for recalculation were 14.3 ± 4.8% for Nb_An33 (n = 12), 13.0 ± 5.1% for ^{99m}Tc-Nb_An33 (n = 12), 35.1 ± 7.1% for ^{99m}Tc-Sestamibi (n = 12) and 12.2 ± 4.7% for Evans Blue.

Blood–brain barrier integrity after microdialysis probe implantation

Possible blood–brain barrier disruption following probe implantation was analysed using two standard compounds for the evaluation of barrier functionality, Evans Blue and ^{99m}Tc-Sestamibi (Dykstra *et al.*, 1992; Staudenherz *et al.*, 2000; Kirton *et al.*, 2002), and our study compound (^{99m}Tc-Nb_An33) in the three experimental rat groups (control rats and *T. b. brucei* AnTat1.1E infected rats at 25–26 dpi and 29–30 dpi). At first, the impact of microdialysis probe implantation on blood–brain barrier integrity was assessed using fluorescence microscopy on brain tissue sections by comparison of Evans Blue extravasation at the ipsi- and contralateral probe side (Figure 1A, pictures 1, 3 and 5 vs. pictures 2, 4 and 6). No significant differences were observed between the ipsilateral and contralateral sides in any of the rat groups, as measured by the MPI of two non-overlapping ROIs (Figure 1A). The effect of microdialysis probe implantation on blood–brain barrier integrity to the two radiolabelled compounds, ^{99m}Tc-Sestamibi and ^{99m}Tc-Nb_An33, was investigated using µSPECT/CT. ^{99m}Tc-tricarbonyl retrodialysis revealed the exact probe dialysis area and transposition of this ROI to the contralateral side defined two ROIs (ipsi- and contralateral ROIs, average size: 5.14 ± 1.07 mm^3) to assess the impact of probe implantation (Figure S1). No significant differences in the brain uptake of ^{99m}Tc-Sestamibi (Figure 1B) and ^{99m}Tc-Nb_An33 (Figure 1C) were observed between the two ROIs in control rats, rats at 25–26 dpi and rats at 29–30 dpi.

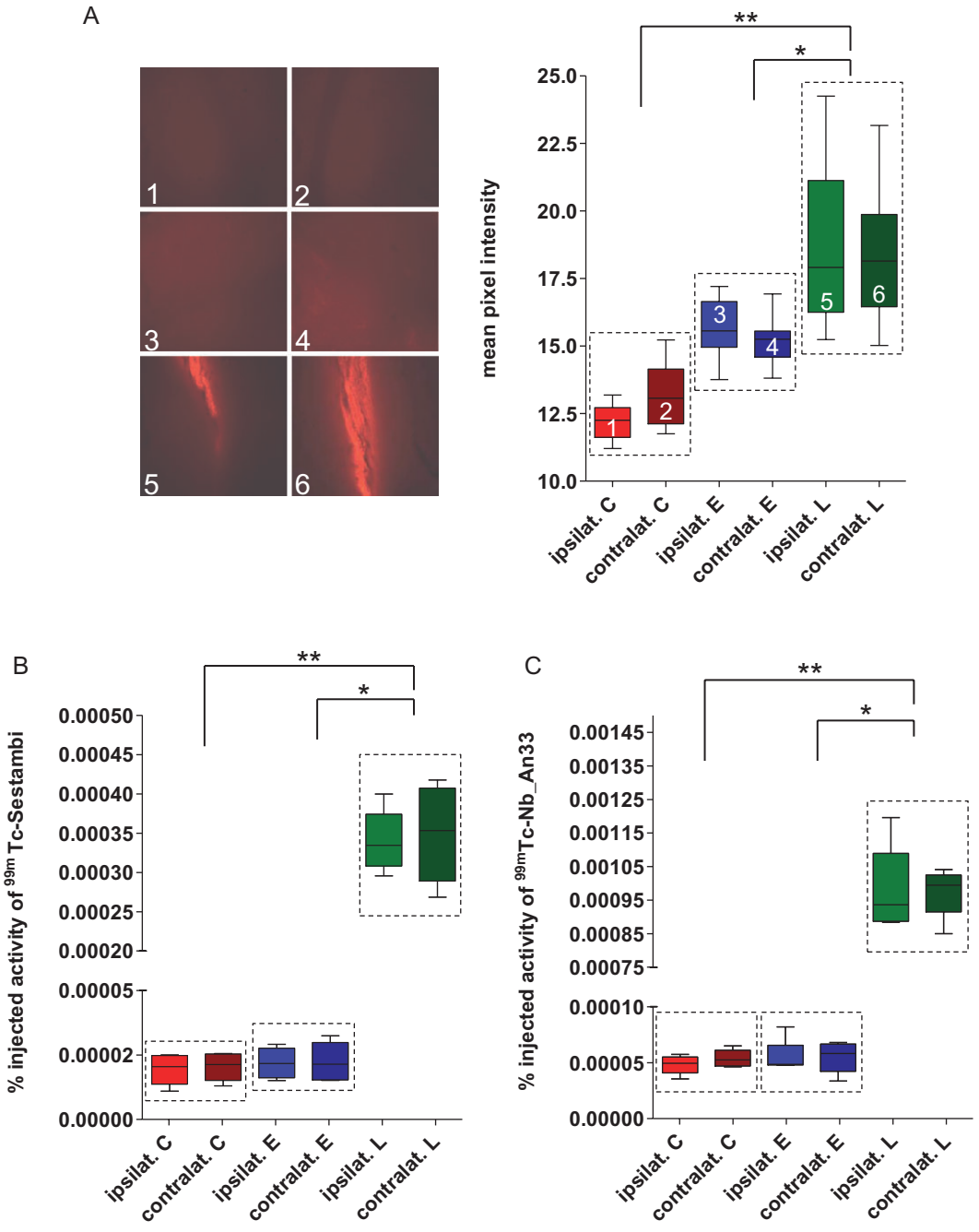

Figure 1

Analysis of the blood–brain barrier integrity after microdialysis probe implantation for the three study compounds (Evans Blue, ^{99m}Tc-Sestamibi and ^{99m}Tc-Nb_An33) in the three experimental rat groups, control rats (C) and *T. b. brucei.* AnTat1.1 infected rats at 25–26 dpi (E) and 29–30 dpi (L). In A, fluorescence microscopic analysis to determine the presence of Evans Blue in brain tissue sections of rats ($n = 6$) subjected to protocol 3. The micrographs are representative of the ipsi- (panels 1, 3 and 5) and contralateral sides (panels 2, 4 and 6) of control rats (panels 1 and 2) and *T. b. brucei.* AnTat1.1 infected rats at 25–26 dpi (pictures 3 and 4) and 29–30 dpi (pictures 5 and 6). Data shown in the bar chart are the mean pixel intensities in the microdialysis area in two non-overlapping ROIs in the ipsi- and contralateral hemispheres determined for at least six tissue slides for each animal. In B, the SPECT image analysis in the ipsi- and contralateral ROI determined upon revealing the microdialysis area (Figure S1) in rats ($n = 4$) that received an i.v. bolus of 122 ± 40 MBq ^{99m}Tc-Sestamibi. Data are expressed as relative to the injected activity (%IA) and relative to the ROI volume (cm^3). In C, SPECT analysis showing the % injected activity cm^{-3} in the ipsi- and contralateral ROI of rats ($n = 4$) that received 119 ± 41 MBq ^{99m}Tc-Nb_An33. Data are shown as box and whisker plots with median, quartiles and ranges. *$P < 0.05$, **$P < 0.01$, significantly different as indicated.

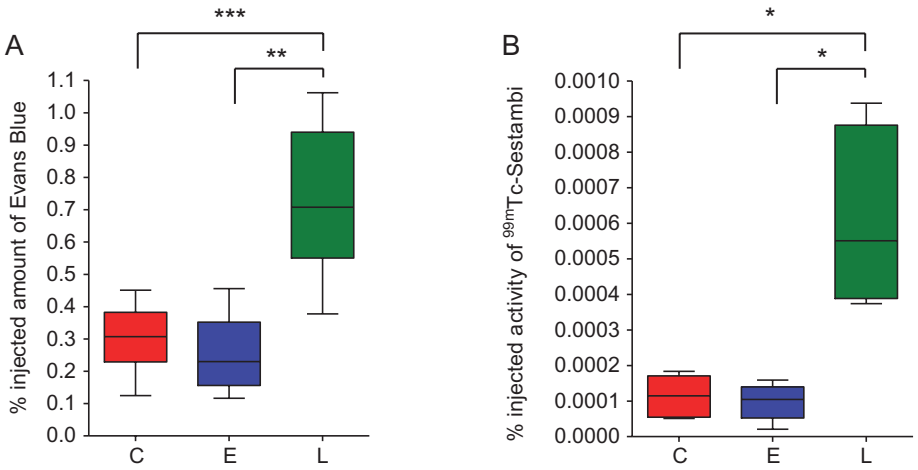

Figure 2

Analysis of the effect of trypanosomiasis on blood–brain barrier integrity: In A, percent recovery of Evans Blue in intracerebral microdialysates obtained from control rats (C) and rats in an early (25–26 dpi; E) and late encephalitic disease stage (29–30 dpi; L) subjected to protocol 3 ((n=13 per group) and after the injection of 2 mL of 0.5% Evans Blue (n = 6 per group). In B, recovery (%) of ^{99m}Tc-Sestamibi in microdialysates within 2 h after i.v. injection of 119 ± 43 MBq (n = 6 per group). Data are shown as box and whisker plots with median, quartiles and ranges. *P < 0.05, **P < 0.01, ***P < 0.001, significantly different as indicated.

Effects of trypanosomiasis on blood–brain barrier integrity

To investigate the effects of trypanosome infection on blood–brain barrier permeability, we compared the CNS accumulation of Evans Blue and ^{99m}Tc-Sestamibi of control rats and rats in an early (25–26 dpi) or late encephalitic disease stage (29–30 dpi). To statistically compare the experimental groups, the results of the ipsilateral and contralateral ROI analyses were pooled for each rat group (see dashed rectangles in Figure 1A,B).

Fluorescence microscopic inspection of the brain slices, collected from rats that were subjected to intracerebral microdialysis (protocol 3), indicated limited Evans Blue penetration from the vasculature in control and 25–26 dpi brains (Figure 1A). The MPI for the control animals and 25–26 dpi animals were not significantly different but in 29–30 dpi rats, a significant increase in Evans Blue fluorescence was observed compared with control (n = 6, P < 0.01,) and 25–26 dpi rats (n = 6, P < 0.05) (Figure 1A). In line with the Evans Blue data, pinhole SPECT/CT analysis also demonstrated a significant increase in brain disposition of ^{99m}Tc-Sestamibi in 29–30 dpi rats, compared with that in control rats (n = 4, P < 0.01) and 25–26 dpi rats (n = 4, P < 0.05) (Figure 1B).

Spectrophotometric analysis of the microdialysates collected following Evans Blue injection confirmed the significant increase (approximate 2.5-fold) in brain uptake in 29–30 dpi rats (n = 13) compared with control rats (P < 0.001; n = 13) and 25–26 dpi rats (P < 0.01; n = 13) (Figure 2A). Similarly, the percentage injected ^{99m}Tc-Sestamibi activity recovered in the microdialysates was increased six-fold in 29–30 dpi animals (n = 6), compared with control rats or 25–26 dpi rats (P < 0.05; each group n = 6) (Figure 2B).

Brain uptake of ^{99m}Tc-Nb_An33 and Nb_An33 in control conditions and during the encephalitic stage of trypanosomiasis

To evaluate the effect of trypanosomiasis on ^{99m}Tc-Nb_An33 perfusion efficiency, pooled ipsi- and contralateral μSPECT/CT image data for each rat group (cf. dashed rectangles in Figure 1C) were compared. All rats showed a limited brain uptake of intact ^{99m}Tc-Nb_An33 but there was more (approximately 20-fold) in the brain of the 29–30 dpi group in comparison with the control group (P < 0.01) and the 25–26 dpi group (P < 0.05). Analysis of ^{99m}Tc-Nb_An33 in the microdialysates also showed a significant, approximately 20-fold increase in the percentage of activity recovered in the dialysates from 29–30 dpi rats when compared with control rats or rats at 25–26 dpi (each n = 7, P < 0.05) (Figure 3A).

Unlabelled Nb_An33 levels were determined by a Nb-specific ELISA in the first two microdialysates from all animals subjected to protocol 3. Brain disposition of Nb_An33 was significantly higher (approximately 3.5-fold) in 29–30 dpi rats, in comparison with control rats or rats at 25–26 dpi (each n = 13, P < 0.01) (Figure 3B). Calculated concentrations of functional Nb_An33 in the hippocampal extracellular fluid, after an i.v. bolus of 4 mg·kg^{-1}, were 50 ± 21 ng·mL^{-1}, 49 ± 26 ng·mL^{-1} and 131 ± 63 ng·mL^{-1} in control animals and rats in the early and late encephalitic stage of trypanosomiasis respectively.

Systemic 99mTc-Nb_An33 and 99mTc-Sestamibi pharmacokinetics

The systemic clearance rates of ^{99m}Tc-Nb_An33 (Figure 4A) and ^{99m}Tc-Sestamibi (Figure 4B) were determined by assessing the blood-pool activity at different time points after i.v. injection. The blood–clearance curves were analysed by non-linear regression and fitted to a two phase exponential decay equa-

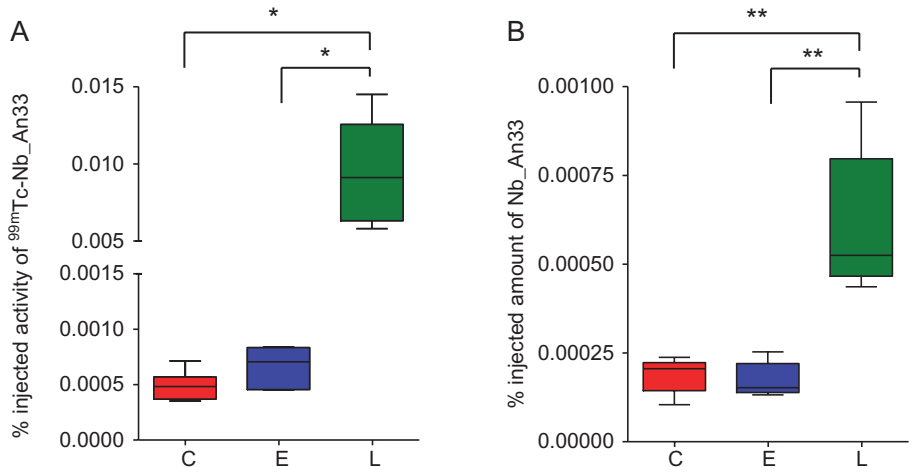

Figure 3

Brain uptake of ^{99m}Tc-Nb_An33 and Nb_An33 in control conditions and during the encephalitic stage of trypanosomiasis: In A, percent recovery of ^{99m}Tc-Nb_An33 in intracerebral microdialysates obtained from control rats(C) and rats in the early (25–26 dpi; E) and late encephalitic disease stage (29–30 dpi; L) ($n = 7$ per group). In B, percent recovery of Nb_An33 based on ELISA in intracerebral microdialysates obtained from the same experimental rat groups after an i.v. bolus of 4 mg·kg^{-1} (n = 13 per group). Data are shown as box and whisker plots with median, quartiles and ranges. *$P < 0.05$, **$P < 0.01$, significantly different as indicated.

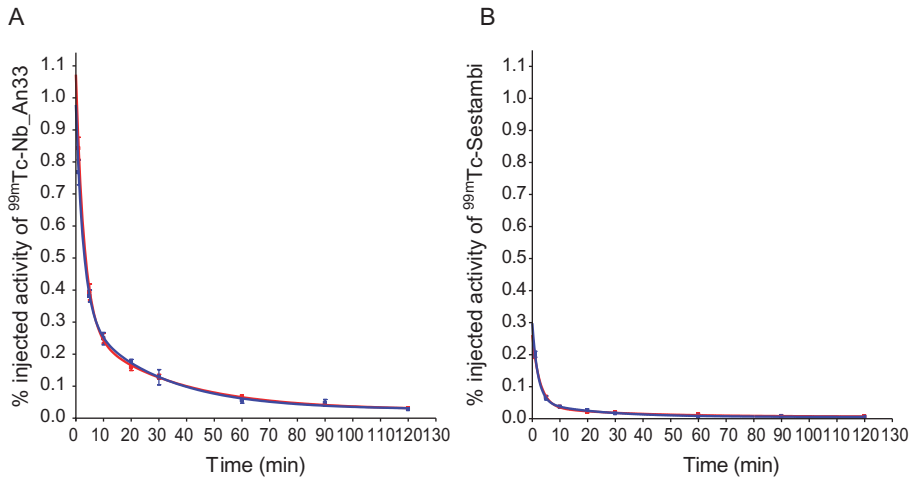

Figure 4

Systemic ^{99m}Tc-Nb_An33 and ^{99m}Tc-Sestamibi pharmacokinetics: Clearance of ^{99m}Tc-Nb_An33 (in A) and ^{99m}Tc-Sestamibi (in B) from total blood of control rats (blue line) and rats at 29–30 dpi (red line) within a 2 h window that corresponds to the microdialysate sampling time. Blood samples were collected from the tail vein at 1, 5, 10, 20, 30, 60, 90 and 120 min post injection of ^{99m}Tc-Nb_An33 (48 ± 20 MBq, $n = 3$ per group) or ^{99m}Tc-Sestamibi (61 ± 45 MBq, $n = 3$ per group). The blood–clearance curves were fitted onto a two phase exponential decay equation. Data shown are mean±SD.

tion (goodness of fit ^{99m}Tc-Nb_An33 curves: control rats R^2 = 0.9832 and 29–30 dpi rats R^2 = 0.9728; goodness of fit ^{99m}Tc-Sestamibi curves: control rats R^2 = 0.9945 and 29–30 dpi rats R^2 = 0.9816). The calculated half-lives for ^{99m}Tc-Nb_An33 for control rats ($T_{1/2}^1$: 1.59 ± 1.07 min; $T_{1/2}^2$: 19.21 ± 10.05 min; $n = 3$) and 29–30 dpi rats ($T_{1/2}^1$: 1.96 ± 1.00 min, $T_{1/2}^2$: 20.02 ± 5.61 min; $n = 3$) were not significantly different (Figure 4A). No significant difference was found between the calculated half-lives for ^{99m}Tc-Sestamibi (Figure 4B) in control rats ($T_{1/2}^1$: 1.74 ± 0.53 min, $T_{1/2}^2$: 19.89 ± 10.28 min; $n = 3$) and 29–30 dpi rats ($T_{1/2}^1$: 1.19 ± 0.66 min, $T_{1/2}^2$: 16.85 ± 8.96 min; $n = 3$). The analysis indicated that both ^{99m}Tc-Nb_An33 and ^{99m}Tc-Sestamibi are rapidly cleared from the blood, with no detectable influence from the infection status.

Discussion and conclusions

In this study, we have evaluated a new method, combining the SPECT technique with intracerebral microdialysis to

assess the permeability of the blood-brain barrier to nanobodies. To date, SPECT has been used to monitor the peripheral biodistribution of nanobodies that are labelled at the hexahistidine tail with ^{99m}Tc. These reports provide evidence for very good target:background biodistribution ratios (Cortez-Retamozo *et al.*, 2002; Gainkam *et al.*, 2008; Vaneycken *et al.*, 2010). However, very limited information is available on the penetration of monovalent nanobodies into the CNS.

Intracerebral microdialysis can provide important data to determine the blood–brain barrier transport characteristics and extracellular/biophase concentrations of a compound (Clinckers *et al.*, 2009). A prerequisite is that the intracerebral implantation of a microdialysis probe does not significantly alter the barrier's physiological and restrictive properties. Several studies have shown a biphasic response in blood–brain barrier permeability, with an increase immediately after probe insertion and a second increase 1–2 days after insertion (Major *et al.*, 1990; Allen *et al.*, 1992; Westergren *et al.*, 1995; Morgan *et al.*, 1996; de Lange *et al.*, 1997; Groothuis *et al.*, 1998). In between these two phases (8-48h after probe insertion), blood–brain barrier functionality seems to be fully restored (Benveniste *et al.*, 1984; Benveniste and Huttemeier, 1990; Clapp-Lilly *et al.*, 1999; Richter *et al.*, 1999), although several parameters should be considered (Grabb *et al.*, 1998). The various shapes, sizes and component materials used for microdialysis sampling can cause a variety of tissue reactions. Also the condition of the parenchyma may affect the response of the blood–brain barrier and the parenchymal tissue to probe implantation. Pathological brain tissue may respond differently to the insertion of a probe in comparison with healthy parenchymal tissue. It is therefore important to carefully analyse the integrity of the barrier function in the system under investigation over the period of time at which samples are collected.

In the present study, the integrity of the blood–brain barrier after implantation of the microdialysis probe was confirmed by fluorescence microscopy. We did not find increased levels of Evans Blue in the vicinity of the probe when comparing brain sections from control animals and animals in the encephalitic stage of trypanosomiasis. These observations are in agreement with data obtained from combined microdialysis and μSPECT/CT using radiolabelled test compounds. We found no difference in the amount of ^{99m}Tc-Sestamibi or ^{99m}Tc-Nb33 between the ipsilateral (i.e. the probe implantation side) and contralateral ROI in both control and infected rats. Clearly, the delay of at least 16h between probe implantation and starting the experimental procedure allowed the blood-brain barrier to recover its normal low permeability, in both healthy and *Trypanosoma*-infected rats. Our experimental procedures allowed the accurate study and quantification of blood–brain barrier function and cerebral uptake of our exogenous test compounds in naive and infected animals. The combined use of intracerebral microdialysis and pinhole μSPECT/CT analysis, moreover, allowed compounds to be recovered in the microdialysate and to be quantified, analysed and tested for activity, thereby providing complementary information to data obtained from μSPECT/CT image analysis.

Using the microdialysis and μSPECT/CT methodologies, either singly or in combination, we also assessed the brain-penetrating potential of Nb_An33, a *T.b. brucei* AnTat1.1 VSG specific nanobody, as a model. Our data demonstrated that, under normal physiological conditions, only a very small proportion (~0.0005%) of the injected Nb_An33 dose entered the brain parenchyma. Microdialysis was a more sensitive assay for these baseline levels than μSPECT/CT. In this context, anaesthesia, needed during the μSPECT/CT procedure, is known to markedly reduce cerebral blood flow (McDowall *et al.*, 1963) and thus to decrease the distribution to the brain of circulating compounds. In the present study, ^{99m}Tc-Nb_An33 was therefore administered to conscious rats, before induction of anaesthesia and μSPECT/CT acquisition. The concentration–time profiles show that by the start of the SPECT recording, more than 70% of the nanobody had been cleared from the circulation. This, in combination with the shorter sampling interval (30 min vs. 120 min), explains why the recovered ^{99m}Tc-Nb_An33 amounts in the image analysis were 10-fold lower than the amounts recovered in the microdialysates. Based on a sensitive Nb_An33-specific ELISA, concentrations of unlabelled Nb_An33 were determined in hippocampal microdialysates collected from non-anaesthetized rats. After correction for the *in vivo* probe recovery, determined by retrodialysis, nanobody concentrations in the brain parenchyma after a 4 mg·kg^{-1} i.v. bolus were calculated to be approximately 50 ng·mL^{-1} under normal physiological conditions. Given that the previously characterized nanobodies require an *in vitro* concentration of ≥0.5 μg·mL^{-1} to cause parasite lysis within 3 h, intracerebral nanobody levels in our experiments were significantly below the anticipated therapeutic levels. This is in agreement with the few publications on non-targeted single domain antibody fragments (Muruganandam *et al.*, 2002; Iqbal *et al.*, 2010). Some receptors on endothelial cells can be targeted by small antigen-binding fragments to allow passage through the blood-brain barrier and to increase intracerebral accumulation. These moieties could be used as barrier-crossing vectors and assembled into chimeric constructs to allow central drug delivery. However, our study highlights that low efficiency passage through the barrier is possible even for non-chimeric nanobodies.

Using the same combination of microdialysis and μSPECT/CT, the passage of our study compounds across the blood–brain-barrier was also evaluated in a rat model of brain inflammation (Darsaud *et al.*, 2003; Chevrier *et al.*, 2005; Amrouni *et al.*, 2010). African trypanosome infection in rats is characterized by two disease stages, similar to those observed in humans: a haemolymphatic and an encephalitic stage where parasites can be detected in the brain parenchyma (Kennedy, 2004; Kristensson *et al.*, 2010). In the late encephalitic phase, there was progressively increasing permeability of the rat blood–brain barrier to sulphorhodamine B (Philip *et al.*, 1994). Also in mice, recent MRI studies have confirmed a significant signal enhancement at 28 days post infection (dpi) (Rodgers *et al.*, 2011). ^{3}[H]-labelled anti-trypanosome drugs (eflornitine, pentamidine and suramin) also attained higher brain levels in mice by 28 dpi (Sanderson *et al.*, 2008; 2009). In spite of these findings in rodents, pentamidine and suramin cannot be used to treat second-stage sleeping sickness patients (see Fairlamb, 2003). Our SPECT and microdialysis results also clearly illustrate that rats, at 29–30 dpi with *T. b. brucei* AnTat1.1E, displayed enhanced blood–brain barrier permeability, compared with their unin-

fected littermates, to ^{99m}Tc-Sestamibi and Evans Blue, yielding increased recovery of Evans Blue and ^{99m}Tc-Sestamibi in microdialysates. Enhanced uptake of Evans Blue was also shown by fluorescence microscopy of brain tissue. These data support the general idea that blood–brain barrier function is progressively disturbed in the late or terminal encephalitic infection stage of trypanosomiasis. The infection-induced defects leading to this compromised barrier function remain to be fully understood (Masocha *et al.*, 2007; Kristensson *et al.*, 2010). Parasite transmigration appeared to occur at the post-capillary venules and, in mice, was, in part, dependent on IFN-γ signalling (Masocha *et al.*, 2004). The increased permeability during late stage trypanosomiasis was not associated with disruption of the tight junctions (Mulenga *et al.*, 2001). However, we found that passage of Evans Blue was only increased 2.5 fold in late stage (29-30 dpi) rats, whereas that of ^{99m}Tc-Sestamibi was increased six-fold, suggesting that the physicochemical properties of compounds still played an important role in the penetration into cerebral tissue, even when the blood–brain barrier was compromised.

Relative to Evans Blue and ^{99m}Tc-Sestamibi, brain disposition of the nanobody ^{99m}Tc-Nb_An33 was even more increased in late encephalitic stage animals, up to 20-fold over the levels in the early encephalitic stage or those in non-infected rats. Theoretically, disease –induced alterations in systemic pharmacokinetics, raising circulating levels of nanobody, could also contribute to the increased brain levels and liver pathology and severe glomerulonephritis are known features of *T. brucei* infection in rodents (Anosa and Kaneko, 1984; van Velthuysen *et al.*, 1994; Magez *et al.*, 2004). However, our pharmacokinetic analysis showed that blood concentrations of ^{99m}Tc-Nb_An-33 were unaffected by disease stage, and thus we can attribute the higher cerebral uptake of ^{99m}Tc-Nb_An33 to increased blood–brain barrier penetration. The same holds true for the enhanced cerebral uptake of ^{99m}Tc-Sestamibi and Evans Blue. In spite of increased blood–brain barrier permeability, the proportion of injected Nb_An33 dose recovered from the brain was still very low. With an i.v. bolus of 4 mg·kg^{-1}, the concentration in the extracellular fluid compartment of the brain of infected animals was approximately 130 ng·mL^{-1}. Given that these concentrations were determined by antigen binding in ELISA, we could unambiguously confirm an increased disposition of active Nb_An33 in late-stage *Trypanosoma*-infected animals.

From our whole blood measurements, we found another factor, rapid clearance from blood, which would contribute to the poor CNS-penetration of the nanobodies. Their very short half-life ($T_{1/2}^1$ < 2 min; $T_{1/2}^2$ ~ 20 min) was probably due to the efficient renal clearance of these low molecular weight (≤15 kDa) proteins (De Groeve *et al.*, 2010; Vaneycken *et al.*, 2010). Adding an anti-albumin domain to create a bivalent construct increased serum half-life (Coppieters *et al.*, 2006) and bivalent constructs with or without a human F_c also displayed significantly prolonged plasma retention (Coppieters *et al.*, 2006; Iqbal *et al.*, 2010). Such F_c-modification of an anti-EGFR/EGFRvIII nanobody allowed its brain tumour imaging potential to be realized (Iqbal *et al.*, 2010). However, the considerably increased molecular weight of bivalent and F_c constructs, compared with monovalent nanobodies might impose restrictions in terms of brain perfusion efficiency. Therefore, CDR loop grafting (Nicaise *et al.*, 2004; Saerens *et al.*, 2005; Vaneycken *et al.*, 2010), onto a yet to be identified scaffold, might yield nanobody formats with a minimal size, required antigen specificity and with beneficial pharmacological and pharmacokinetic properties for passage into the CNS.

In conclusion, we have demonstrated that nanobodies, using Nb_An33 as model molecule, were able to cross the blood–brain barrier at a detectable level. In addition, in an experimental model of CNS inflammation, passage of nanobodies across this barrier was increased. However, the systemic pharmacokinetics of monovalent nanobodies, overall, do not favour the accumulation in brain of therapeutically relevant concentrations, even in animals with cerebral inflammation. We therefore suggest that efforts should be undertaken to modify these nanobodies to yield improved brain penetrating properties without losing their beneficial size. To quantitatively study the penetration into the CNS of new constructs *in vivo*, intracerebral microdialysis represents a powerful and sensitive technique.

Acknowledgements

We acknowledge the excellent technical assistance of Cindy Peleman, laboratory technician at the In Vivo Cellular and Molecular Imaging lab of the VUB. This work was also supported by the kind technical assistance of Ella Omasta, Maria Slazak and Marie-Thérèse Detobel of the Cellular and Molecular Immunology Unit at VUB and Susana Santos and João Silva Duarte of the Department of Pharmaceutical Chemistry and Drug Analysis at VUB. We thank Cathy Jensen of the department of Neurology at the University hospital UZ Brussel for editing the manuscript. Ralph Clinckers is a post-doctoral fellow of the Fund for Scientific Research-Flanders (FWO Vlaanderen). Guy Caljon is a post-doctoral fellow supported by the InterUniversity Attraction Poles Programme (IAP, P6/15) of the Belgian Science Policy. Tony Lahoutte is a Senior Clinical Investigator of the Research Foundation – Flanders (Belgium) (FWO). The research at ICMI is funded by the Interuniversity Attraction Poles Program (P6/38).

Conflicts of interest

The authors state no conflict of interest.

References

Abulrob A, Sprong H, Van Bergen En Henegouwen P, Stanimirovic D (2005). The blood-brain barrier transmigrating single domain antibody: mechanisms of transport and antigenic epitopes in human brain endothelial cells. J Neurochem 95: 1201–1214.

Allen DD, Crooks PA, Yokel RA (1992). 4-Trimethylammonium antipyrine: a quaternary ammonium nonradionuclide marker for blood-brain barrier integrity during *in vivo* microdialysis. J Pharmacol Toxicol Methods 28: 129–135.

Amin DN, Rottenberg ME, Thomsen AR, Mumba D, Fenger C, Kristensson K *et al.* (2009). Expression and role of CXCL10 during the encephalitic stage of experimental and clinical African trypanosomiasis. J Infect Dis 200: 1556–1565.

Amrouni D, Gautier-Sauvigné S, Meiller A, Vincendeau P, Bouteille B, Buguet A *et al.* (2010). Cerebral and peripheral changes occurring in nitric oxide (NO) synthesis in a rat model of sleeping sickness: identification of brain iNOS expressing cells. PLoS One 5: e9211. doi:10.1371/journal.pone.0009211.

Anosa VO, Kaneko JJ (1984). Pathogenesis of *Trypanosoma brucei* infection in deer mice (*Peromyscus maniculatus*). Ultrastructural pathology of the spleen, liver, heart, and kidney. Vet Pathol 21: 229–237.

Auffret CA, Turner MJ (1981). Variant specific antigens of *Trypanosoma brucei* exist in solution as glycoprotein dimers. Biochem J 193: 647–650.

Baral TN, Magez S, Stijlemans B, Conrath K, Vanhollebeke B, Pays E *et al.* (2006). Experimental therapy of African trypanosomiasis with a nanobody-conjugated human trypanolytic factor. Nat Med 12: 580–584.

Barry JD, Mcculloch R (2001). Antigenic variation in trypanosomes: enhanced phenotypic variation in a eukaryotic parasite. Adv Parasitol 49: 1–70.

Benveniste H, Huttemeier PC (1990). Microdialysis–theory and application. Prog Neurobiol 35: 195–215.

Benveniste H, Drejer J, Schousboe A, Diemer NH (1984). Elevation of the extracellular concentrations of glutamate and aspartate in rat hippocampus during transient cerebral ischemia monitored by intracerebral microdialysis. J Neurochem 43: 1369–1374.

Chevrier C, Canini F, Darsaud A, Cespuglio R, Buguet A, Bourdon L (2005). Clinical assessment of the entry into neurological state in rat experimental African trypanosomiasis. Acta Trop 95: 33–39.

Clapp-Lilly KL, Roberts RC, Duffy LK, Irons KP, Hu Y, Drew KL (1999). An ultrastructural analysis of tissue surrounding a microdialysis probe. J Neurosci Methods 90: 129–142.

Clinckers R, Smolders I, Vermoesen K, Michotte Y, Danhof M, Voskuyl R *et al.* (2009). Prediction of antiepileptic drug efficacy: the use of intracerebral microdialysis to monitor biophase concentrations. Expert Opin Drug Metab Toxicol 5: 1267–1277.

Conrath KE, Lauwereys M, Galleni M, Matagne A, Frere JM, Kinne J *et al.* (2001). Beta-lactamase inhibitors derived from single-domain antibody fragments elicited in the camelidae. Antimicrob Agents Chemother 45: 2807–2812.

Coppieters K, Dreier T, Silence K, De Haard H, Lauwereys M, Casteels P *et al.* (2006). Formatted anti-tumor necrosis factor alpha VHH proteins derived from camelids show superior potency and targeting to inflamed joints in a murine model of collagen-induced arthritis. Arthritis Rheum 54: 1856–1866.

Cortez-Retamozo V, Lauwereys M, Hassanzadeh Gh G, Gobert M, Conrath K, Muyldermans S *et al.* (2002). Efficient tumor targeting by single-domain antibody fragments of camels. Int J Cancer 98: 456–462.

Cross GA (1975). Identification, purification and properties of clone-specific glycoprotein antigens constituting the surface coat of *Trypanosoma brucei*. Parasitology 71: 393–417.

Darsaud A, Bourdon L, Chevrier C, Keita M, Bouteille B, Queyroy A *et al.* (2003). Clinical follow-up in the rat experimental model of African trypanosomiasis. Exp Biol Med (Maywood) 228: 1355–1362.

De Groeve K, Deschacht N, De Koninck C, Caveliers V, Lahoutte T, Devoogdt N *et al.* (2010). Nanobodies as tools for *in vivo* imaging of specific immune cell types. J Nucl Med 51: 782–789.

De Lange EC, Danhof M, De Boer AG, Breimer DD (1997). Methodological considerations of intracerebral microdialysis in pharmacokinetic studies on drug transport across the blood-brain barrier. Brain Res Brain Res Rev 25: 27–49.

Dykstra KH, Hsiao JK, Morrison PF, Bungay PM, Mefford IN, Scully MM *et al.* (1992). Quantitative examination of tissue concentration profiles associated with microdialysis. J Neurochem 58: 931–940.

Fairlamb AH (2003). Chemotherapy of human African trypanosomiasis: current and future prospects. Trends Parasitol 19: 488–494.

Gainkam LO, Huang L, Caveliers V, Keyaerts M, Hernot S, Vaneycken I *et al.* (2008). Comparison of the biodistribution and tumor targeting of two 99mTc-labeled anti-EGFR nanobodies in mice, using pinhole SPECT/micro-CT. J Nucl Med 49: 788–795.

Grabb MC, Sciotti VM, Gidday JM, Cohen SA, Van Wylen DG (1998). Neurochemical and morphological responses to acutely and chronically implanted brain microdialysis probes. J Neurosci Methods 82: 25–34.

Groothuis DR, Ward S, Schlageter KE, Itskovich AC, Schwerin SC, Allen CV *et al.* (1998). Changes in blood-brain barrier permeability associated with insertion of brain cannulas and microdialysis probes. Brain Res 803: 218–230.

Hamers-Casterman C, Atarhouch T, Muyldermans S, Robinson G, Hamers C, Songa EB *et al.* (1993). Naturally occurring antibodies devoid of light chains. Nature 363: 446–448.

Hernot S, Cosyns B, Droogmans S, Garbar C, Couck P, Vanhove C *et al.* (2010). Effect of high-intensity ultrasound-targeted microbubble destruction on perfusion and function of the rat heart assessed by pinhole-gated SPECT. Ultrasound Med Biol 36: 158–165.

Huang L, Gainkam LO, Caveliers V, Vanhove C, Keyaerts M, De Baetselier P *et al.* (2008). SPECT imaging with 99mTc-labeled EGFR-specific nanobody for in vivo monitoring of EGFR expression. Mol Imaging Biol 10: 167–175.

Iqbal U, Trojahn U, Albaghdadi H, Zhang J, O'connor-Mccourt M, Stanimirovic D *et al.* (2010). Kinetic analysis of novel mono- and multivalent VHH-fragments and their application for molecular imaging of brain tumours. Br J Pharmacol 160: 1016–1028.

Kennedy PG (2004). Human African trypanosomiasis of the CNS: current issues and challenges. J Clin Invest 113: 496–504.

Kirton A, Kloiber R, Rigel J, Wolff J (2002). Evaluation of pediatric CNS malignancies with (99m)Tc-methoxyisobutylisonitrile SPECT. J Nucl Med 43: 1438–1443.

Kristensson K, Nygard M, Bertini G, Bentivoglio M (2010). African trypanosome infections of the nervous system: parasite entry and effects on sleep and synaptic functions. Prog Neurobiol 91: 152–171.

Lanham SM, Godfrey DG (1970). Isolation of salivarian trypanosomes from man and other mammals using DEAE-cellulose. Exp Parasitol 28: 521–534.

Lauwereys M, Arbabi Ghahroudi M, Desmyter A, Kinne J, Holzer W, De Genst E *et al.* (1998). Potent enzyme inhibitors derived from dromedary heavy-chain antibodies. EMBO J 17: 3512–3520.

Lee HB, Blaufox MD (1985). Blood volume in the rat. J Nucl Med 26: 72–76.

Loening, AM, Gambhir SS (2003). AMIDE: a free software tool for multimodality medical image analysis. Mol Imaging, 2: 131–137.

Magez S, Truyens C, Merimi M, Radwanska M, Stijlemans B, Brouckaert P *et al*. (2004). P75 tumor necrosis factor-receptor shedding occurs as a protective host response during African trypanosomiasis. J Infect Dis 189: 527–539.

Major O, Shdanova T, Duffek L, Nagy Z (1990). Continuous monitoring of blood-brain barrier opening to Cr51-EDTA by microdialysis following probe injury. Acta Neurochir Suppl (Wien) 51: 46–48.

Masocha W, Robertson B, Rottenberg ME, Mhlanga J, Sorokin L, Kristensson K (2004). Cerebral vessel laminins and IFN-gamma define *Trypanosoma brucei brucei* penetration of the blood-brain barrier. J Clin Invest 114: 689–694.

Masocha W, Rottenberg ME, Kristensson K (2007). Migration of African trypanosomes across the blood-brain barrier. Physiol Behav 92: 110–114.

Mcdowall DG, Harper AM, Jacobson I (1963). Cerebral blood flow during halothane anaesthesia. Br J Anaesth 35: 394–402.

Meikle SR, Kench P, Kassiou M, Banati RB (2005). Small animal SPECT and its place in the matrix of molecular imaging technologies. Phys Med Biol 50: R45–R61.

Morgan ME, Singhal D, Anderson BD (1996). Quantitative assessment of blood-brain barrier damage during microdialysis. J Pharmacol Exp Ther 277: 1167–1176.

Mulenga C, Mhlanga JD, Kristensson K, Robertson B (2001). *Trypanosoma brucei brucei* crosses the blood-brain barrier while tight junction proteins are preserved in a rat chronic disease model. Neuropathol Appl Neurobiol 27: 77–85.

Muruganandam A, Tanha J, Narang S, Stanimirovic D (2002). Selection of phage-displayed llama single-domain antibodies that transmigrate across human blood-brain barrier endothelium. FASEB J 16: 240–242.

Nguyen VK, Desmyter A, Muyldermans S (2001). Functional heavy-chain antibodies in *Camelidae*. Adv Immunol 79: 261–296.

Nicaise M, Valerio-Lepiniec M, Minard P, Desmadril M (2004). Affinity transfer by CDR grafting on a nonimmunoglobulin scaffold. Protein Sci 13: 1882–1891.

Nikolskaia OV, De ALaP KYV, Lonsdale-Eccles JD, Fukuma T, Scharfstein J *et al*. (2006). Blood-brain barrier traversal by African trypanosomes requires calcium signaling induced by parasite cysteine protease. J Clin Invest 116: 2739–2747.

Paxinos G, Watson C (1986). The Rat Brain in Stereotaxic Coordinates. Academic: San Diego, CA.

Philip KA, Dascombe MJ, Fraser PA, Pentreath VW (1994). Blood-brain barrier damage in experimental African trypanosomiasis. Ann Trop Med Parasitol 88: 607–616.

Priotto G, Kasparian S, Mutombo W, Ngouama D, Ghorashian S, Arnold U *et al*. (2009). Nifurtimox-eflornithine combination therapy for second-stage African *Trypanosoma brucei gambiense* trypanosomiasis: a multicentre, randomised, phase III, non-inferiority trial. Lancet 374: 56–64.

Richter DW, Schmidt-Garcon P, Pierrefiche O, Bischoff AM, Lalley PM (1999). Neurotransmitters and neuromodulators controlling the hypoxic respiratory response in anaesthetized cats. J Physiol 514 (Pt 2): 567–578.

Rodgers J (2010). Trypanosomiasis and the brain. Parasitology 137: 1995–2006.

Rodgers J, Mccabe C, Gettinby G, Bradley B, Condon B, Kennedy PG (2011). Magnetic resonance imaging to assess blood-brain barrier damage in murine trypanosomiasis. Am J Trop Med Hyg 84: 344–350.

Saerens D, Pellis M, Loris R, Pardon E, Dumoulin M, Matagne A *et al*. (2005). Identification of a universal VHH framework to graft non-canonical antigen-binding loops of camel single-domain antibodies. J Mol Biol 352: 597–607.

Saerens D, Stijlemans B, Baral TN, Nguyen Thi GT, Wernery U, Magez S *et al*. (2008). Parallel selection of multiple anti-infectome Nanobodies without access to purified antigens. J Immunol Methods 329: 138–150.

Sanderson L, Dogruel M, Rodgers J, Bradley B, Thomas SA (2008). The blood-brain barrier significantly limits eflornithine entry into *Trypanosoma brucei brucei* infected mouse brain. J Neurochem 107: 1136–1146.

Sanderson L, Dogruel M, Rodgers J, De Koning HP, Thomas SA (2009). Pentamidine movement across the murine blood-brain and blood-cerebrospinal fluid barriers: effect of trypanosome infection, combination therapy, P-glycoprotein, and multidrug resistance-associated protein. J Pharmacol Exp Ther 329: 967–977.

Schultzberg M, Ambatsis M, Samuelsson EB, Kristensson K, Van Meirvenne N (1988). Spread of *Trypanosoma brucei* to the nervous system: early attack on circumventricular organs and sensory ganglia. J Neurosci Res 21: 56–61.

Staudenherz A, Fazeny B, Marosi C, Nasel C, Hoffmann M, Puig S *et al*. (2000). Does (99m)Tc-Sestamibi in high-grade malignant brain tumors reflect blood-brain barrier damage only? Neuroimage 12: 109–111.

Stijlemans B, Conrath K, Cortez-Retamozo V, Van Xong H, Wyns L, Senter P *et al*. (2004). Efficient targeting of conserved cryptic epitopes of infectious agents by single domain antibodies. African trypanosomes as paradigm. J Biol Chem 279: 1256–1261.

Stijlemans B, Caljon G, Natesan SKA, Conrath K, Skepper J, Pérez-Morga D *et al*. (2011). High affinity Nanobodies against the *Trypanosoma brucei* VSG are potent trypanolytic agents that block endocytosis. PLoS Pathog 7: e1002072.

Trickler WJ, Miller DW (2003). Use of osmotic agents in microdialysis studies to improve the recovery of macromolecules. J Pharm Sci 92: 1419–1427.

Van Velthuysen ML, Mayen AE, Van Rooijen N, Fleuren GJ, De Heer E, Bruijn JA (1994). T cells and macrophages in *Trypanosoma brucei*-related glomerulopathy. Infect Immun 62: 3230–3235.

Vaneycken I, Govaert J, Vincke C, Caveliers V, Lahoutte T, De Baetselier P *et al*. (2010). *In vitro* analysis and *in vivo* tumor targeting of a humanized, grafted nanobody in mice using pinhole SPECT/micro-CT. J Nucl Med 51: 1099–1106.

Vanhamme L, Lecordier L, Pays E (2001). Control and function of the bloodstream variant surface glycoprotein expression sites in *Trypanosoma brucei*. Int J Parasitol 31: 523–531.

Vanhove C, Defrise M, Bossuyt A, Lahoutte T (2009). Improved quantification in single-pinhole and multiple-pinhole SPECT using micro-CT information. Eur J Nucl Med Mol Imaging 36: 1049–1063.

Wang Y, Wong SL, Sawchuk RJ (1993). Microdialysis calibration using retrodialysis and zero-net flux: application to a study of the distribution of zidovudine to rabbit cerebrospinal fluid and thalamus. Pharm Res 10: 1411–1419.

Westergren I, Nystrom B, Hamberger A, Johansson BB (1995). Intracerebral dialysis and the blood-brain barrier. J Neurochem 64: 229–234.

Yun O, Priotto G, Tong J, Flevaud L, Chappuis F (2010). NECT is next: implementing the new drug combination therapy for *Trypanosoma brucei gambiense* sleeping sickness. PloS Negl Trop Dis 4: e720.

Zamze SE, Ashford DA, Wooten EW, Rademacher TW, Dwek RA (1991). Structural characterization of the asparagine-linked oligosaccharides from *Trypanosoma brucei* type II and type III variant surface glycoproteins. J Biol Chem 266: 20244–20261.

Supporting information

Additional Supporting Information may be found in the online version of this article:

Figure S1 Ipsilateral and contralateral ROI identification during the combined μSPECT and intracerebral microdialysis experiments to determine the impact of probe implantation: (A) SPECT image of the head region of a rat subjected to protocol 2 with ^{99m}Tc-Nb_An33 as test compound (122 ± 40 MBq i.v.); (B) unveiling the exact probe localization by retrodialysis of approximately 185 MBq ^{99m}Tc-tricarbonyl; (C) identification of a three-dimensional ROI corresponding to the microdialysis area; (D) radioactivity count determination within the ROI prior to the ^{99m}Tc-tricarbonyl retrodialysis; (E) transposition of the same ROI to the contralateral side to determine radioactivity counts in the brain region without probe implant; (F) sagittal SPECT image view with indication of the ROI position.

Please note: Wiley-Blackwell are not responsible for the content or functionality of any supporting materials supplied by the authors. Any queries (other than missing material) should be directed to the corresponding author for the article.